Journal of
Manufacturing and Materials Processing

Article

Laser Tracker-Based on-the-Fly Machine Tool Calibration without Real-Time Synchronization

Mark P. Sanders [1,*], Matthias Bodenbenner [1], Philipp Dahlem [1], Dominik Emonts [1], Benjamin Montavon [1] and Robert H. Schmitt [1,2]

[1] Laboratory for Machine Tools and Production Engineering (WZL), RWTH Aachen University, Campus-Boulevard 30, 52074 Aachen, Germany
[2] Fraunhofer Institute for Production Technology IPT, Steinbachstraße 17, 52074 Aachen, Germany
* Correspondence: m.sanders@wzl-mq.rwth-aachen.de

Abstract: Consistent high volumetric performance of machine tools is an essential requirement for high-quality machining. Periodic machine tool calibration ensures said performance and allows for timely corrective actions preventing scrap or rework. Reducing the duration of the calibration process decreases associated cost through non-productive downtime and allows for data acquisition in thermal real-time. The authors enhance an indirect calibration method based on measuring points within the machine volume using a laser tracker by removing the necessity for standstill. To circumvent requiring high fidelity space and time synchronization between metrology system and machine tool, only deviations perpendicular to the path are considered. To do so, the 3D laser tracker data are rotationally transformed such that one axis aligns with the motion direction and can subsequently be omitted as input data for the system of equations solving for geometric errors. Due to the absence of unique measurement-point-to-machine-point mapping, data alignment between nominal path and measurement data is proposed as an iterative alignment process of points to path. The method is tested simulatively and experimentally. It demonstrated conformity to the simulation as well as to the pre-existing calibration method based on laser trackers and shows good agreement with the direct calibration device API XD Laser.

Keywords: machine tool calibration; laser tracker; on-the-fly

Citation: Sanders, M.P.; Bodenbenner, M.; Dahlem, P.; Emonts, D.; Montavon, B.; Schmitt, R.H. Laser Tracker-Based on-the-Fly Machine Tool Calibration without Real-Time Synchronization. *J. Manuf. Mater. Process.* **2023**, *7*, 60. https://doi.org/10.3390/jmmp7020060

Academic Editors: Bruce L. Tai and ChaBum Lee

Received: 19 January 2023
Revised: 24 February 2023
Accepted: 26 February 2023
Published: 7 March 2023

Copyright: © 2023 by the authors. Licensee MDPI, Basel, Switzerland. This article is an open access article distributed under the terms and conditions of the Creative Commons Attribution (CC BY) license (https://creativecommons.org/licenses/by/4.0/).

1. Introduction

Faster machine tool calibration can allow for more frequent calibration at the same cost due to reduced machine down time, metrology equipment cost, and operator cost per calibration or simply reduce calibration effort [1,2].

Machine tool calibration methods can be separated into direct calibration methods and indirect calibration methods. With direct calibration methods, the calibration measurands—per-axis error motions—are measured directly. Examples are API XD Laser™; Renishaw XM-60™, XM-600™, and XL-60™; SIOS SP 5000™ and SP 15000™; and Status Pro µLine™ [1,3].

An additional differentiation can be made regarding measurement principle: Laser-based methods take advantage of linear light propagation and constant, well-known laser wavelength. With material-based methods, measurements are performed in relation to reference artifacts. Gravity-based methods use earth's gravitational field as reference. Most commercially available, modern, calibration devices are based on laser interferometry for distance measurements and additional components for lateral and rotational displacement measurements, e.g., additional laser beams, optics, PSDs, inclinometers, etc. [1,3–5].

With indirect calibration methods, derived quantities are measured in the machine volume and inverse mathematical models for computing per axis error motions are employed. The advantages of indirect calibration methods are, generally, shorter overall calibration duration and less effortful overall measurement setup due to measuring multiple axes simultaneously. Material-based indirect calibration methods can take advantage of machine-integrated (touch) probe systems. Examples are SAMBA [6] or (dynamic) R-Tests [7,8]. Laser-based indirect calibration methods may rely solely on interferometric length measurement with multiple fixed laser beams, e.g., Etalon LineCal® or step diagonal measurements [9,10]. Other approaches use multilateration for position measurement based on laser distance measurements, e.g., Etalon LaserTracer® or see references [11,12].

Laser trackers use absolute distance measurements and rotational encoders to determine 3D target positions, which in turn can be used as the data basis for machine tool calibration, see [13–15].

On-the-fly (OTF) calibration stands for an indirect calibration process with the machine in motion not requiring machine standstill to measure data [12]. To be able to compare actual measurements of any quantity changing with machine position to ideal data within the machine control system, existing calibration methods require precise data synchronization between the calibration system and machine control system. With a slow, exemplary machine velocity of 1000 mm/min a time shift between ideal machine position and measured data of only 1 ms results in an error of 17 µm in motion direction. With unknown machine control motion parameters for velocity ramps, acceleration and jerk values, and dynamic machine errors, a posteriori 1:1 target and actual position data mapping is infeasible. Hence, existing on-the-fly calibration systems require direct access to machine control data [12].

Based on the calibration model published by Montavon et al. in [14], a model allowing for on-the-fly measurement was developed. The main concept is to only take deviations perpendicular to a predefined path (see Figure 1) into account to avoid requiring time synchronization.

1.1. Requirements and a Priori Assumptions

The novel calibration method relies on the following assumptions. For modern precision machine tools these requirements are generally satisfied.

- Rigid body behavior of the machine under test: The mathematical model is based on rigid body assumptions. Hence, machine errors resulting from non-rigid-body behavior may cause errors in analysis.
- Volumetric and geometric errors and their spatial gradients are generally small in magnitude compared to overall machining volume.
- Negligible dynamic path deviations perpendicular to a path in linear, steady motion: For the proposed method to work, the machine under test must not exhibit relevant additional errors creating path deviations compared to a load-free standstill case. For milling or turning machines this assumption generally holds true, as this requirement equally applies to workpiece machining.
- Negligible backlash error contributions: In the current state of the calibration model backlash errors (or different errors for axes forward and backward direction) are not considered. Backlash errors could be considered in future implementations, see Section 3. Discussion.

1.2. Description of Calibration Steps in Detail

In addition to the calibration steps of Montavon et al. in [14], the authors add modifications allowing for on-the-fly use in certain key areas (see Table 1). The following subsections detail the described calibration steps.

Table 1. Comparison of the calibration steps in [14] and in the approach described in this publication.

<table>
<tr><th>Fast Machine Tool Calibration Using a Single Laser Tracker [14]</th><th>Novel OTF Approach</th></tr>
<tr><td>Random points distributed within machine's working volume; requires overdetermined system of equations (SoE) via number of random points (similar to Figure 2)</td><td>Continuous path in machine's working volume enabling differentiating error influences (see Figure 1)</td></tr>
<tr><td colspan="2">Data acquisition with laser tracker</td></tr>
<tr><td>Standstill recognition</td><td>Continuous path data</td></tr>
<tr><td>Data alignment using rigid transformation (Kabsch/Procrustes) [16,17]</td><td>Rough alignment using fixed points and centroid; iterative fine alignment points to corresponding path position</td></tr>
<tr><td>Setup SoE using rigid body model (RBM) and volumetric errors</td><td>Setup SoE using RBM and path deviations</td></tr>
<tr><td>Weight SoE components according to measurement uncertainty</td><td>Rotate SoE components such that one SoE entry per 3D datum points in path direction and ignore component in path direction for SoE; weight rest according to measurement uncertainty</td></tr>
<tr><td colspan="2">Solve SoE for error table entries</td></tr>
</table>

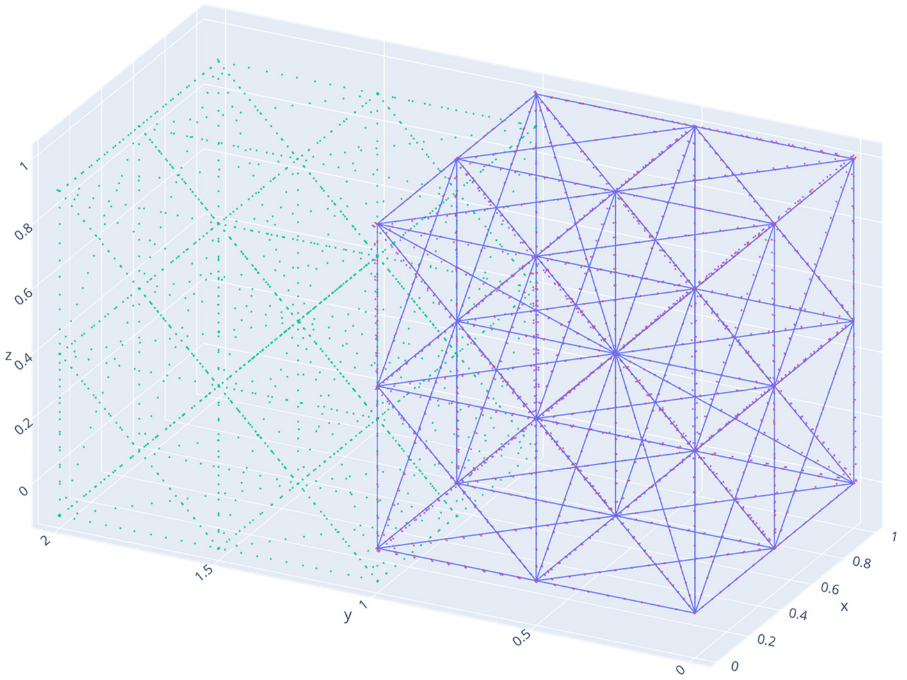

Figure 1. Simulated exemplary OTF calibration path (blue, continuous) and simulated laser tracker measurements points (green). Note the shift and rotation (by 90°) between both shapes demonstrating the different coordinate systems of laser tracker and machine. Red points show simulated measurement points after rough alignment.

1.2.1. Path Creation

With the developed OTF method as the input data, there must be enough information to (ideally) unambiguously discern geometric errors. Due to the concept of not taking information on path direction into account, there is no full volumetric error information available at each point on the path, as is with some other indirect calibration methods [1,6,7,12,18]. Hence, path-planning algorithms as calibration preparations must consider said fact and ensure discernability. A path containing multiple face and space diagonals can fulfil those requirements (blue line in Figure 1).

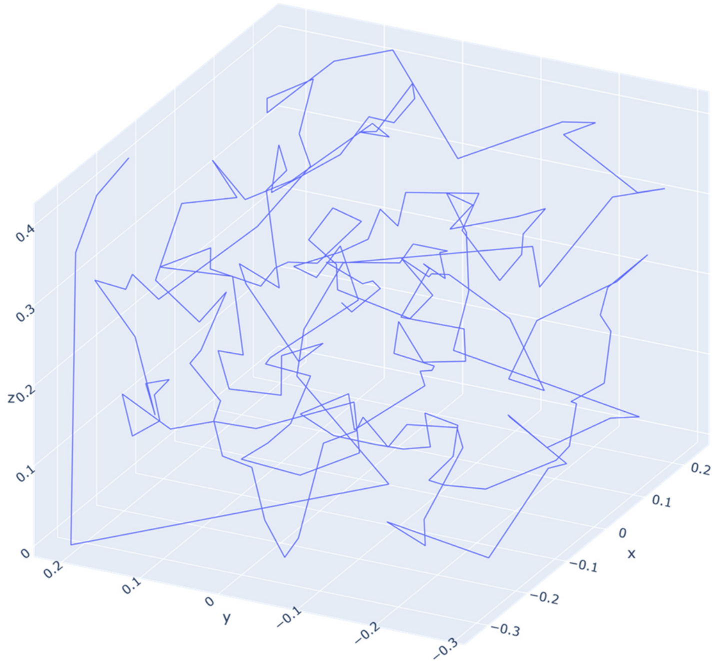

Figure 2. Reference trajectory to compare standstill laser tracker calibration with OTF calibration on (grid axis unit: [m]).

1.2.2. Data Acquisition

At the trajectory's start point, recording of a continuous data stream of laser-tracking data with 500 points/s is started until the end of the trajectory. The laser tracker is set up affixed to the machine's workpiece table. Tilting of the machine due to weight shift through moving axes assemblies should not influence calibration.

1.2.3. Alignment

With [14] a coordinate system alignment is possible via conventional rigid fit algorithms (Kabsch/Procrustes) [16,17] working on equally sized sets of measured and ideal points. Alignment of laser tracker data to a continuous path is more challenging than with standstill points because the possibility to uniquely map the measured points to target points that the machine moved to is lacking; However, as input data for the SoE, only deviations are necessary, so the acquired laser tracker data must be transformed into the machine coordinate system and only relative errors are taken into account. Hence, a two-step alignment process is proposed and tested.

To roughly align the measured data to the path, some unique characteristics easily found in the measured data and path are exploited: start point, end point, and centroid. First, measured points are transformed translationally such that the start point of the measured data coincides with the start point in the machine coordinate system (MCS). Rough rotational transformation is performed by rotating all measured points around the start point such that the centroid and the end point in the measured data best align to said points in the trajectory data. Thus, the start and end point must not coincide. See red points in Figure 1.

For fine alignment, an iterative process is employed. For a fixed number of steps or until the stop criterion for diminishing relative improvement is reached, for all measurement points the closest corresponding point on the path is calculated and then a rigid fit alignment between measured points and calculated closest points on the path is executed. Thus, the measurement points are all translated and rotated to better align to the path iteratively.

Points close to direction changes in the trajectory are not included due to a possibly erroneous mapping between the target and the nominal data and assumed larger dynamic/control errors.

1.2.4. System of Equations

The basic system of equations (see $\hat{V}_{(3\cdot n\times 1)}$; $\hat{\mathbf{M}}_{(3\cdot n\times 3\cdot n)}$; $\cdot\hat{\mathbf{B}}_{3\cdot n\times u}$; $\cdot U^{*}_{(u\times 1)}$ in [14]) is created according to Montavon et al. with entries for each measured point in the aligned data instead. For nominal position data, for SoE setup the respective closest points on the path are used. Hence, the volumetric errors used as input are perpendicular deviations between the nominal and actual path; input deviation between the nominal and actual in path direction is always zero. The basic SoE is then extended according to the following equations in Sections 1.2.5 and 1.2.6.

1.2.5. Coordinate Transformations and Weights

Montavon et al. [14] described a weight matrix $\hat{\boldsymbol{W}}$ in their algorithm composed as a block diagonal matrix of 3 × 3 submatrices $\boldsymbol{W_i}$, which weight the equation components according to measurement uncertainty.

In the approach outlined in this article, the authors modify the existing approach to suit the needs for OTF calibration: Instead of calculating a weight for each of n total data points and its coordinates from uncertainty and covariance only, first a coordinate rotation into a point-individual path coordinate system (PCS) is conducted (see Figure 3). This allows for ignoring all data on path direction and only considering deviations perpendicular to the trajectory. Without time synchronization, the current actual point on the path cannot be matched to the current nominal point on the path, but perpendicular path deviations can still be used for calibration. For said COS, the first axis for each measurement $\boldsymbol{a_{i,1}}$ is defined as the path direction for the current point (normalized). The second axis $\boldsymbol{a_{i,2}}$ defining said coordinate system is defined as the portion of the laser tracker beam direction perpendicular to the first axis (normalized), if existing, and the third axis $\boldsymbol{a_{i,3}}$ perpendicular to both other axes. If the first axis is pointing in the beam direction, any two other axes can be chosen perpendicular to one another (see also Figure 3). If the beam direction is not equal to the path direction for measurement $\boldsymbol{i}$ with measured point $\boldsymbol{p_{i,\ MCS}}$ in MCS, the path COS axes are defined according to the following equations with laser beam direction in MCS $\boldsymbol{b_{i,\ MCS}}$, and path direction $\boldsymbol{d_{i,\ MCS}}$:

$$a_{i,1} = \frac{d_{i,\ MCS}}{|d_{i,\ MCS}|};\quad a_{i,2} = \frac{b_{i,\ MCS} - b_{i,\ MCS}\cdot a_{i,1}}{|b_{i,\ MCS} - b_{i,\ MCS}\cdot a_{i,1}|}\ ;\quad a_{i,3} = a_{i,1}\times a_{i,2} \tag{1}$$

The rotation from MCS to PCS $\boldsymbol{P_i}$ can then be denoted as:

$$\boldsymbol{P_i}_{\ (3\times 3)} = \begin{pmatrix} a_{i,1}^{T} \\ a_{i,2}^{T} \\ a_{i,3}^{T} \end{pmatrix} \tag{2}$$

An overall coordinate transformation matrix $\hat{\boldsymbol{P}}$ is concatenated from all individual transformation matrices $\boldsymbol{P_i}$:

$$\hat{\boldsymbol{P}}_{(3\cdot n\times 3\cdot n)} = \begin{pmatrix} P_1 & \cdots & 0 \\ \vdots & \ddots & \vdots \\ 0 & \cdots & P_n \end{pmatrix} \tag{3}$$

Weights have to be determined in PCS with the weight in path direction equals zero. Weights for the other components can be calculated using uncertainty contributions in respective directions for the laser tracker; in beam direction uncertainty is generally lower, hence said component should be weighted more. Hence entries for $\boldsymbol{W_i}$ are set as reciprocals of measurement standard deviation approximations squared for the respective measurement direction. U_{beam} and U_{radial} are approximate uncertainty values for measurement in beam direction and perpendicular to beam direction. In path coordinate system weights for each line in the SoE can then be defined as a diagonal matrix $\boldsymbol{W_i}$ with the $\boldsymbol{W_{i\ 1,1}}$ entry being zero.

$$\begin{gathered} W_{i\ 2,2} = \frac{1}{\sqrt{U_{beam}^2 \cdot \left(a_{i,2} \cdot d_{i,MCS}\right)^2 + U_{radial}^2 \cdot \left(1 - \left(a_{i,2} \cdot d_{i,MCS}\right)^2\right)}} \\ W_{i\ 3,3} = \frac{1}{\sqrt{U_{beam}^2 \cdot \left(a_{i,3} \cdot d_{i,MCS}\right)^2 + U_{radial}^2 \cdot \left(1 - \left(a_{i,3} \cdot d_{i,MCS}\right)^2\right)}} \\ \boldsymbol{W_i} = \begin{pmatrix} 0 & 0 & 0 \\ 0 & W_{i\ 2,2} & 0 \\ 0 & 0 & W_{i\ 3,3} \end{pmatrix} \end{gathered} \tag{4}$$

An overall weight matrix $\hat{\boldsymbol{W}}$ is constructed as block diagonal matrix.

$$\hat{\boldsymbol{W}}_{(3 \cdot n \times 3 \cdot n)} = \begin{pmatrix} W_1 & \cdots & 0 \\ \vdots & \ddots & \vdots \\ 0 & \cdots & W_n \end{pmatrix} \tag{5}$$

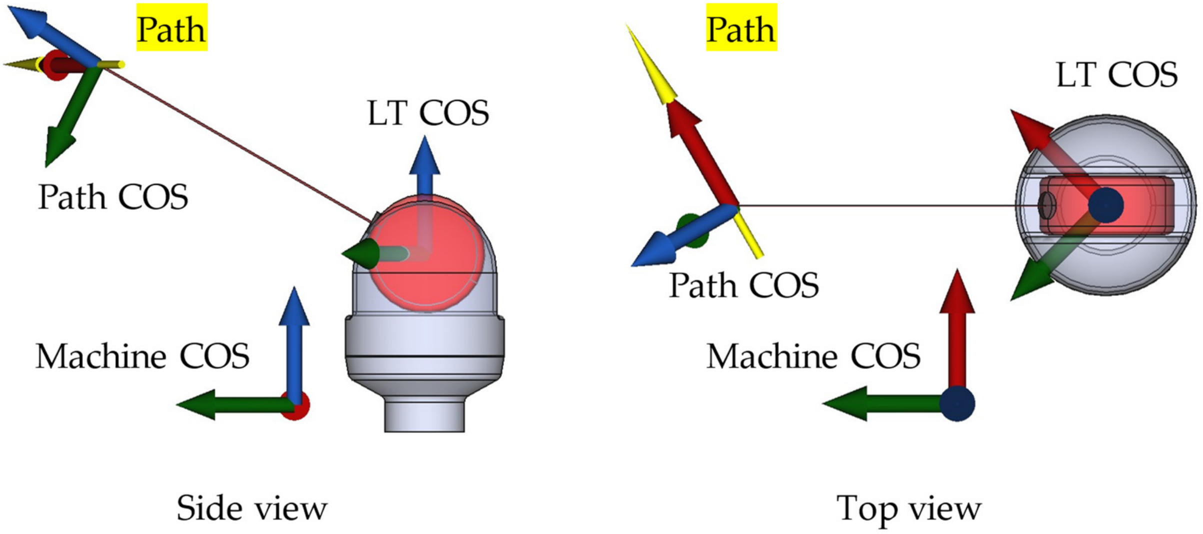

Figure 3. Exemplary depiction of a path coordinate system as defined in Section 1.2.5. Due to the weight approach depicted in this section, for each point a path coordinate system (PCS) must be defined, such that one coordinate axis points in the direction of the machine path/movement. The second coordinate axis is defined to point as much in laser direction as possible, while being perpendicular to the first axis. The third axis is defined by being perpendicular to both previous axes and defining a right-handed COS.

1.2.6. Solving for Geometric Errors

With all components an overall SoE can be constructed based on the overall SoE described by Montavon et al. [14] (see $\hat{\boldsymbol{V}}$, $\hat{\mathbf{M}}$, $\cdot\,\hat{\mathbf{B}}$, $\cdot\,\boldsymbol{U}^*$) and the respective $\hat{\boldsymbol{P}}$ and $\hat{\boldsymbol{W}}$ matrices (Equations (3) and (6)).

$$\hat{\mathbf{W}} \cdot \hat{\boldsymbol{P}} \cdot \hat{\boldsymbol{V}} = \hat{\mathbf{W}} \cdot \hat{\boldsymbol{P}} \cdot \hat{\mathbf{M}} \cdot \hat{\mathbf{B}} \cdot \boldsymbol{U}^* \tag{6}$$

The said SoE can be solved with a least square approach respectively using the Moore–Penrose pseudoinverse (†):

$$\boldsymbol{U}_{opt}^* = \left(\hat{\mathbf{W}} \cdot \hat{\boldsymbol{P}} \cdot \hat{\mathbf{M}} \cdot \hat{\mathbf{B}}\right)^\dagger \cdot \ \hat{\mathbf{W}} \cdot \hat{\boldsymbol{P}} \cdot \hat{\boldsymbol{V}} \tag{7}$$

1.2.7. Uncertainty Computation

To compute the covariance matrices $\boldsymbol{Cov}_{\boldsymbol{cart,\ i}}$, the covariance matrices for uncertainty in spherical coordinates $\boldsymbol{Cov}_{\boldsymbol{sph,\ i}}$ are used and transformed to cartesian coordinates. It is assumed standard deviation perpendicular to beam is equal in elevation and azimuth.

$$\boldsymbol{Cov}_{\boldsymbol{sph,\ i}} = \begin{pmatrix} U_{beam}^2 & 0 & 0 \\ 0 & U_{radial}^2 & 0 \\ 0 & 0 & U_{radial}^2 \end{pmatrix} \tag{8}$$

With the Jacobian matrix for transformation from spherical coordinates to cartesian coordinates $\boldsymbol{J}_{\boldsymbol{sph,i}}$, the covariance matrix for each measrued point $\boldsymbol{Cov}_{\boldsymbol{cart,\ i}}$ is calculated as follows.

$$\boldsymbol{J}_{\boldsymbol{sph,i}} = \begin{pmatrix} -sin(\varphi_i) \cdot cos(\theta_i) & -r_i \cdot cos(\varphi_i) \cdot cos(\theta) & r_i \cdot sin(\varphi_i) \cdot sin(\theta_i) \\ cos(\varphi_i) \cdot cos(\theta_i) & -r_i \cdot sin(\varphi_i) \cdot cos(\theta) & -r_i \cdot cos(\varphi_i) \cdot sin(\theta_i) \\ sin(\theta_i) & 0 & r_i \cdot cos(\theta_i) \end{pmatrix} \tag{9}$$

$$\boldsymbol{Cov}_{\boldsymbol{cart,\ i}} = \boldsymbol{J}_{\boldsymbol{sph,i}} \cdot \boldsymbol{Cov}_{\boldsymbol{sph,i}} \cdot \boldsymbol{J}_{\boldsymbol{sph,i}}^{\boldsymbol{T}} \tag{10}$$

$$\hat{\mathbf{C}}_{(3\cdot n\times 3\cdot n)} = \begin{pmatrix} \boldsymbol{Cov}_{\boldsymbol{cart,\ 1}} & \cdots & 0 \\ \vdots & \ddots & \vdots \\ 0 & \cdots & \boldsymbol{Cov}_{\boldsymbol{cart,n}} \end{pmatrix} \tag{11}$$

Based on the results from the previous matrix inversion, according to the guide to the expression of uncertainty in measurement (GUM) [19,20] the covariance and respective uncertainties for axis error computation can be determined:

$$\mathbf{Cov}\left(\boldsymbol{U}_{\boldsymbol{opt}}^{*}\right) = \left(\hat{\mathbf{W}} \cdot \hat{\boldsymbol{P}} \cdot \hat{\mathbf{M}} \cdot \hat{\mathbf{B}}\right)^{\dagger} \cdot \hat{\mathbf{W}} \cdot \hat{\boldsymbol{P}} \cdot \hat{\mathbf{C}} \cdot \hat{\boldsymbol{P}}^{\boldsymbol{T}} \cdot \hat{\mathbf{W}}^{\boldsymbol{T}} \cdot \left[\left(\hat{\mathbf{W}} \cdot \hat{\boldsymbol{P}} \cdot \hat{\mathbf{M}} \cdot \hat{\mathbf{B}}\right)^{\dagger}\right]^{\boldsymbol{T}} \tag{12}$$

The diagonal entries of $\mathbf{Cov}\left(\boldsymbol{U}_{\boldsymbol{opt}}^{*}\right)$ are the individual uncertainty values for entries in U_{opt}^{*}.

2. Validation

Validation of the described method is separated into multiple steps.

First, the calibration method is validated simulatively against error vector data created using an exemplary error table and an implementation of rigid body model (see Figure 4 for simulative results).

Experimental OTF data are acquired in a machine tool using a path shown in Figure 1. Resulting data are fed into the OTF calibration method. Standstill points at machine volume edges and at 150 random locations in machine volume are acquired and fed into the calibration algorithm by Montavon et al. [14]. At 200 different points in machine volume, reference standstill data are collected (Uncomp. Meas. in Figure 5). The output error table data of both Montavon et al.'s calibration model and the OTF calibration method are used to predict volumetric errors at the reference data points in machine volume.

In addition to data acquired in the former experiment, machine error motions are measured using a direct machine tool calibration approach with the calibration device API XD Laser with a 6D calibration head. Individual error motion tables are compared.

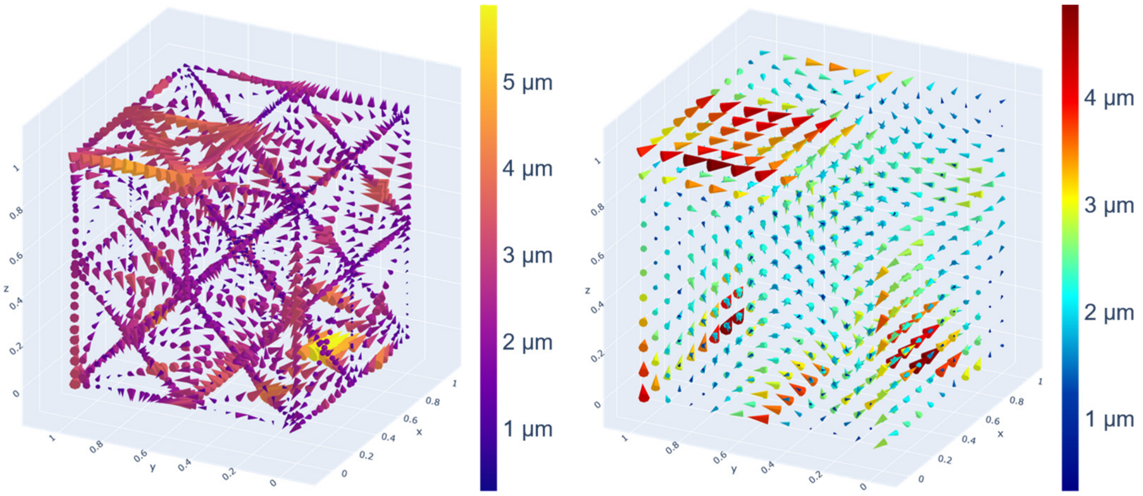

Figure 4. (**Left side**) shows simulated residual deviations on path, right shows residual volumetric errors on a regular grid (grid axis unit: [m]). Larger deviations seem to occur in areas of ambiguity: residuals generally larger in path direction can be seen on the (**left side**).

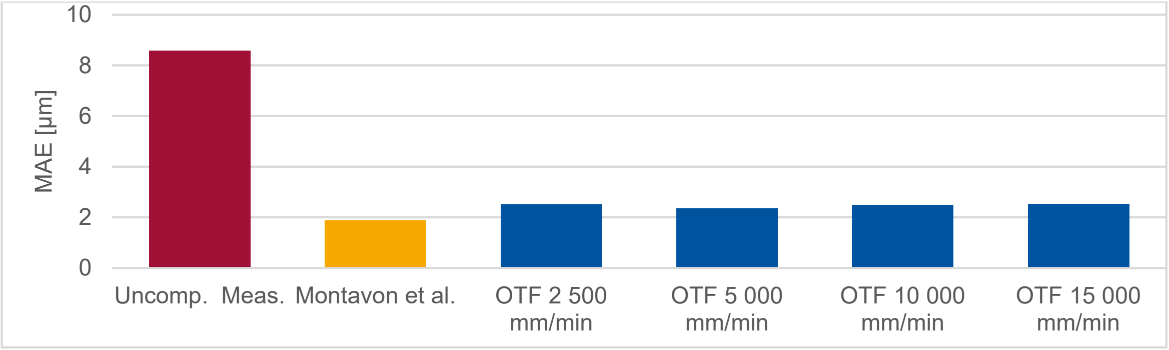

Figure 5. Volumetric error prediction comparison with different methods on a random set of points. Uncomp. Meas. shows the mean absolute error (MAE) vector length over all reference points. Montavon et al. [14] shows the mean absolute error between the measured points and their prediction using standstill calibration method. The OTF bars show MAE for OTF calibration with different velocities.

2.1. Simulative Validation

As a first step in testing the described calibration method, a simulative validation approach is taken. By simulating volumetric errors in a machine volume, simulating laser tracker measurement along a path within said volume, and trying to replicate the volumetric error data, the approach is tested theoretically. This is summarized as:

1. Create a path for OTF calibration.
2. Create a random error table for a simulated machine tool.
3. Select a number of points on the path.
4. Compute perpendicular volumetric errors using RBM along points on the path.
5. Translate and rotate the points + error vectors into an arbitrary coordinate system to simulate measurement with a laser tracker.
6. Align measurement points to the ideal path as described in Sections 1.2.3–1.2.5.
7. Compute respective error vectors in machine coordinate system.
8. Calculate error tables using aforementioned data.
9. Test error prediction:
    1. Self-test: on the path simulated errors should be replicated.

2. Grid test: on a regular point grid within the machine's working volume simulated errors should be replicated.

The simulation showed a good prediction on the path. The mean absolute error for path deviation was reduced by ca. 99% from 117 µm to 0.95 µm. Additionally, the volumetric error prediction was tested on a regular grid with simulated volumetric errors through a rigid body model. Prediction showed also satisfactory results on said regular grid with mean volumetric errors two orders of magnitude smaller than original errors. The mean absolute error over all volumetric error vectors could be reduced by 99% from 103 µm to 0.87 µm. See Figure 4 for simulative validation.

2.2. Experimental Validation—Comparison to Montavon et al. [14]

As the next validation step, the OTF calibration method is compared to the laser tracker-based calibration method using standstill points.

With the machine tool under test, for the standstill method 226 calibration points are measured with the laser tracker. In standstill, 200 additional reference points are measured to be used to compare with error prediction. The OTF calibration method trajectory is run with four different machine velocities between 2 500 mm/min and 15 000 mm/min, to compare the method with data acquired at different machine speeds. See Table 2.

Table 2. Machine trajectories in chronological order.

Trajectory (Chronologically Ordered)	Duration
OTF 2500 mm/min	24 min
Montavon et al. calibration method [14]	18 min
OTF 10,000 mm/min	5.5 min
OTF 5000 mm/min	10 min
Reference Points (see Figure 2)	15 min
OTF 15,000 mm/min	4 min

Compensation tables were created from all calibration runs. The calculated compensation tables were used as input for a rigid body model to predict the volumetric errors at the reference standstill points. The mean absolute residual between predicted and measured reference points was calculated and is shown in Figure 5. The overall magnitude of geometric errors is quite small with the Spinner U5-630 machine tool. All residual errors include influences of different error sources: All methods are influenced equally by machine repeatability, backlash errors, and non-rigid-body-behavior of the machine tool. The overall measurement time frame is 83 min, the spindle is not running and the trajectories consist of steady, straight-line paths. Hence, thermal drift is assumed to be an insignificant influence. The same applies to dynamic and control errors. Hence, differences in residual errors must stem from errors introduced due to calibration methods and different laser tracker uncertainty in standstill compared to dynamic measurement. Machine velocity does not seem to influence calibration uncertainty significantly. In direct comparison, calibration with standstill has a slightly lower residual error (0.5 µm lower MAE) at the cost of slower calibration measurement.

2.3. Experimental Validation against Direct Measuring System API XD Laser

Finally, the OTF method is compared to a state-of-the-art direct measuring machine tool calibration device, the API XD Laser, which is capable of measuring up to six error parameters per axis in a single setup. As a measurement setup parameter, a machine velocity of 2500 mm/min is used, resulting in a time spent on path of 19 min. The SMR target is moved from the bird bath to a magnetic holder at the spindle without interrupting the laser beam to achieve relative interferometric distance measurements with low uncertainty. Data were recorded as described above resulting in more than 500,000 points measured along the path. After data reduction, mean filtering data, and excluding corners, 4427 3D values were used as $\hat{V}$ input for the SoE.

2.3.1. Individual Error Motion Result Discussion

Figures 6–8 show exemplary positioning, straightness and rotational errors measured with an API XD Laser and with the OTF calibration method. The following conventions for error table are applied: Positioning errors and rotational errors are set to zero at the axes' zero positions, if applicable, or alternatively at the minimum position available for both measurements. Straightness errors are set to zero at the zero position, if applicable, or at the minimum position and the maximum position available for both measurements. Conventions can be applied for calibration data and later compensation without actually changing the machine behavior. Said conventions allow for better comparison between error tables in general, and here especially for both calibration methods.

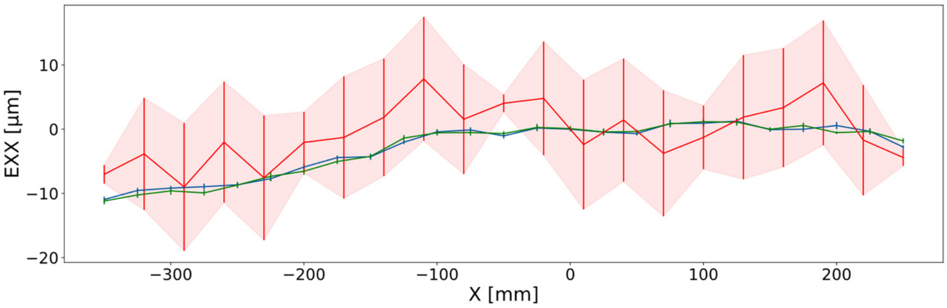

Figure 6. EXX error as an exemplary positioning error. Blue/green are forward/backward values for API XD Laser measurements with respective error bars computed from values over five measurement runs. Red is OTF laser tracker measurements with respective computed uncertainty area.

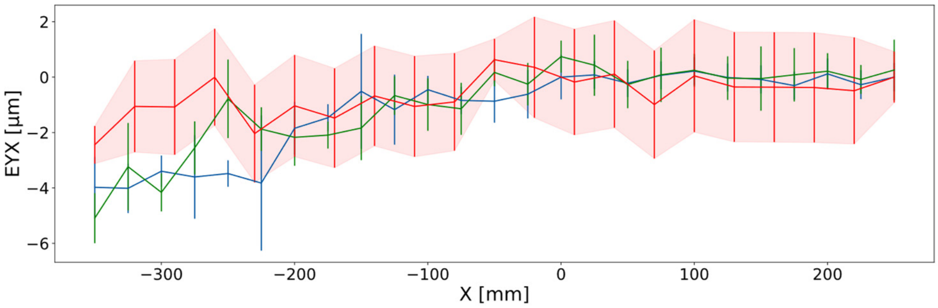

Figure 7. EYX error. Blue/green are forward/backward values for API XD Laser measurements with respective error bars computed from values over five measurement runs. Red is OTF laser tracker measurements with respective computed uncertainty area.

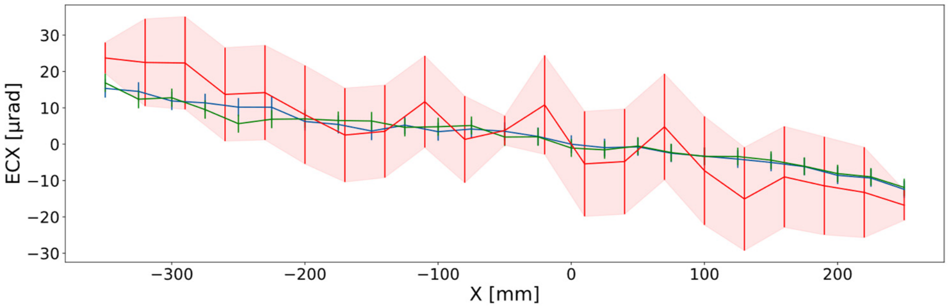

Figure 8. ECX error. Blue/green are forward/backward values for API XD Laser measurements with respective error bars computed from values over five measurement runs. Red is OTF laser tracker measurements with respective computed uncertainty area.

The OTF calibration method can analyze positioning error with less than ca. 10 µm deviation from the API XD Laser measurement over the whole axis range (see Figure 6 and Appendix A). Due to the limitation of not considering data on motion direction, the positioning error data can only be inferred mathematically from path deviation data on diagonal paths and paths perpendicular to the axes' directions (e.g., straight lines in Y and Z for X axis, of which there are only a few: at the start, end, and middle of the axis). Hence, residual errors and uncertainty is larger than for straightness errors.

For straightness errors, path deviation can be quite directly converted into error data, hence calculated uncertainty as well as experimental deviation from directly measured error data is lower (less than 5 µm for all errors—see Figure 7 and Appendix A).

Rotational error deviation between both measurements is in the range of up to 25 µrad (see Figure 8 and Appendix A). With indirect calibration methods like OTF, rotational errors are calculated using volumetric error data. Thus, the rotational error measurement deviation between the XD Laser and OTF calibration multiplied with the maximum rotational lever arm should be in a similar order of magnitude as the straightness deviations. With a maximum measured axis length of 600 mm and, thus, a maximum lever arm (half the axis length) of 300 mm, this assumption roughly holds true ($300\ \text{mm} \cdot 25\ \mu\text{m/m} = 7.5\ \mu\text{m}$).

Overall, residual errors are in the order of magnitude of laser tracker uncertainty. The results do not indicate significant additional errors due to calibration model errors or rigid body model assumption but also cannot rule out said influences.

2.3.2. Overall Evaluation

Finally, with data from the XD Laser and from OTF calibration, volumetric error vectors on a grid were computed and compared (see Figure 9). For comparison, squareness errors were not taken into account, as only two of the three squareness errors were measured with the API XD Laser setups. To compare errors the following conventions were applied to the error tables (see Appendix A): For positioning and rotational errors, the values were set to zero at the 0 position, if applicable, or at the minimum API XD Laser position. For straightness errors, the tables were set to zero at the minimum axis position and the slope value minimum to maximum point measured with the API XD Laser was subtracted from all points. Using the resulting error tables, volumetric errors on a regular grid with the size of the axes' ranges measured with the API XD Laser were computed.

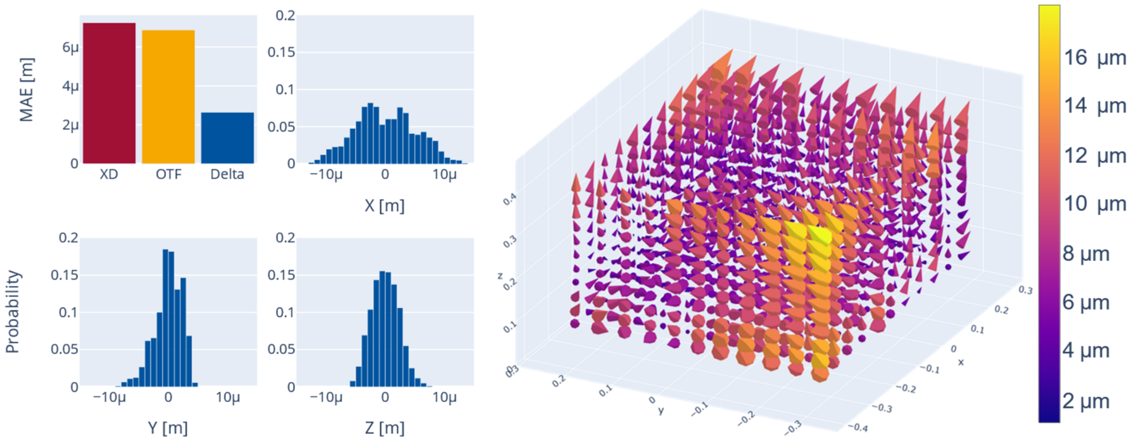

Figure 9. (**Top left**): Mean absolute error on a regular grid calculated using error table data from XD Laser, OTF calibration with a RBM, and the MAE of the delta between both. Please note the magnitude of errors. (**Left**): Histograms showing relative probability for volumetric error deviations in X/Y/Z on a grid between XD Laser measurement and OTF calibration. (**Right**): Difference visualized as cone plot on the regular grid (grid axis unit: [m]).

The methods showed mean absolute errors of 7.2 µm and 6.9 µm, respectively. As a comparison, both volumetric errors were subtracted from each other, resulting in a mean absolute deviation of 2.65 µm.

3. Discussion

The novel calibration method described in this article showed promising results simulatively, hence said method was proven to be mathematically sound against a different implementation of a rigid body model (see [21]) which in turn is validated against the SIEMENS VCS RBM. Simulatively and experimentally it was able to predict errors with residual errors close to those exhibited by a calibration method using standstill points [14].

It delivered single error table data with residual errors compared to a direct measuring system (API XD Laser) in the order of single microns.

While showing micron level residual errors, this method is still not as accurate as more traditional direct and indirect calibration methods, which can achieve sub-micron uncertainties, which is not possible with this method. The OTF method relies on laser tracker measurements, which in turn rely on rotational encoder-based measurements which limit the overall accuracy. For smaller modern precision machine tools, the uncertainty this method delivers could be insufficient depending on the intended machining application.

With larger machine tools, error magnitude generally increases while measurement setup effort for direct measuring machine tool calibration also increases. Hence, for larger machine tools with bigger errors, this calibration method can deliver sufficient measurement accuracy with greatly reduced measurement effort, duration, and resulting cost.

Currently, the method is only implemented for three axis machine tools and backlash errors are not calculated. Both are current implementation limitations, which could be included in the future. Backlash errors could either be implemented as a fixed directional error contribution per error (little additional data requirements) or as forward/backward error tables, which would double the number of unknown variables.

The method described in this article is significantly faster than other calibration methods which do not allow for OTF measurements. As thermal errors can change significantly in the order of minutes, faster calibration methods are preferred to acquire training or validation data thermal machine tool error models.

4. Conclusions and Outlook

A new laser tracker-based calibration method was developed which allows for on-the-fly machine tool calibration while circumventing the requirement for real-time and low jitter machine tool/laser tracker synchronization. Via per point coordinate transformation only perpendicular path deviations can be taken into account as input data for calibration. Hence, a special trajectory in the machine volume has been proposed to still be able to acquire data for all axes error parameters as well as adapted laser tracker/machine tool coordinate system alignment methods. The calibration method was validated simulatively and experimentally and showed promising results with calibration errors in the order of laser tracker uncertainty (a few micrometers) compared to the API XD Laser. Due to less standstill, calibration for three linear axes can be performed for the exemplary machine tool Spinner U5-630 in under 10 min, thus close to or in thermal real-time.

In the current form, backlash errors are not considered. There are two ways to include backlash which can be tested in the future: One is in a simplified way, only allowing for a single backlash error parameter per error motion, hence, adding 14 additional unknown variables. Alternatively, full backlash errors can be considered with forward and backward error tables for each error motion, resulting in double the overall number of unknown variables to solve for and respective information requirement to be fulfilled with measurement data. Support for five-axis calibration could be added in the future but is not yet included. Covariances (Equations (8)–(10)) are approximated using fixed standard deviation values but uncertainty computation can be improved by either inferring standard deviation from measurement data directly or with a more sophisticated laser tracker uncertainty model.

Author Contributions: Conceptualization, M.P.S., M.B. and P.D.; Methodology, M.P.S., P.D. and B.M.; Software, M.P.S. and M.B.; Validation, M.P.S.; Investigation, M.P.S.; Resources, M.B.; Data curation, M.B.; Writing—original draft, M.P.S.; Writing—review & editing, D.E. and B.M.; Visualization, M.P.S.; Supervision, D.E., B.M. and R.H.S.; Project administration, D.E. and B.M.; Funding acquisition, P.D., B.M. and R.H.S. All authors have read and agreed to the published version of the manuscript.

Funding: Funded by the Deutsche Forschungsgemeinschaft (DFG, German Research Foundation) under Germany's Excellence Strategy—EXC-2023 Internet of Production—390621612 and funded by the Deutsche Forschungsgemeinschaft (DFG, German Research Foundation)—298597595.

Data Availability Statement: Not available.

Conflicts of Interest: The authors declare no conflict of interest.

Appendix A

Shown below are all error graphs for a thorough comparison. Positioning errors and rotational errors are set to zero at the axes' zero positions, if applicable, or alternatively at the minimum position available for both measurements. Straightness errors are set to zero at the zero position, if applicable, or at the minimum position and the maximum position available for both measurements. Blue/green are forward/backward values for API XD Laser measurements with respective error bars computed from values over five measurement runs. Red is laser tracker measurements with respective computed uncertainty area.

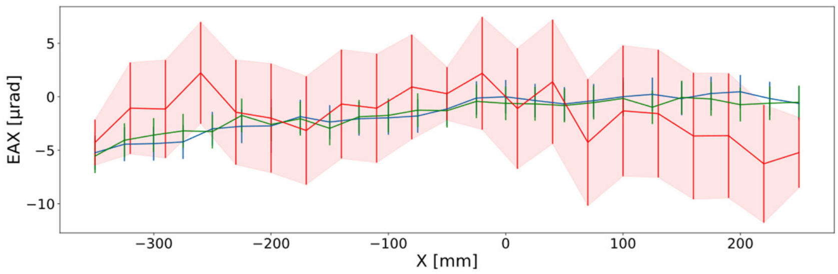

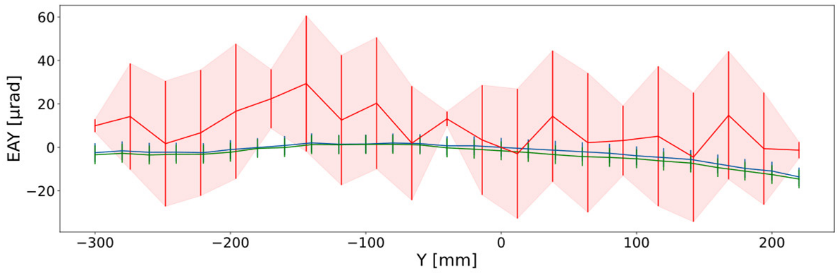

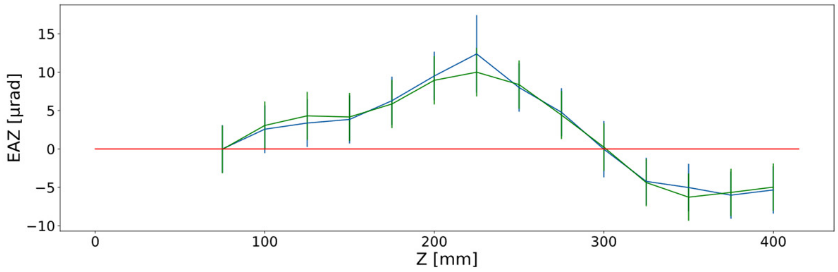

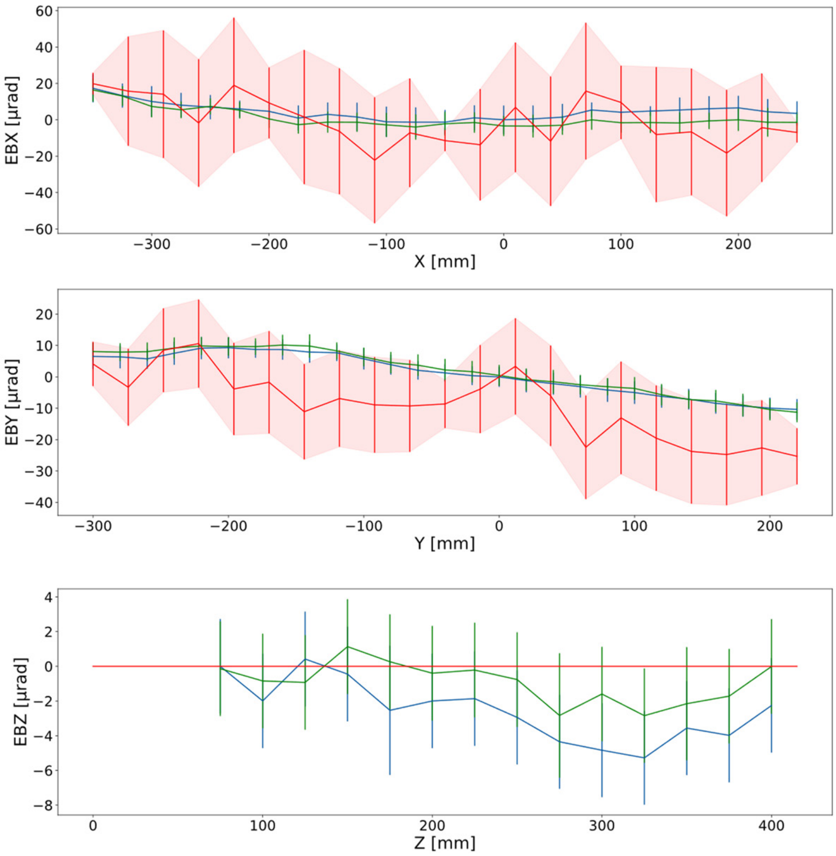
EBX [µrad]
60
40
20
0
−20
−40
−60
−300
−200
−100
0
100
200
X [mm]
EBY [µrad]
20
10
0
−10
−20
−30
−40
−300
−200
−100
0
100
200
Y [mm]
EBZ [µrad]
4
2
0
−2
−4
−6
−8
0
100
200
300
400
Z [mm]

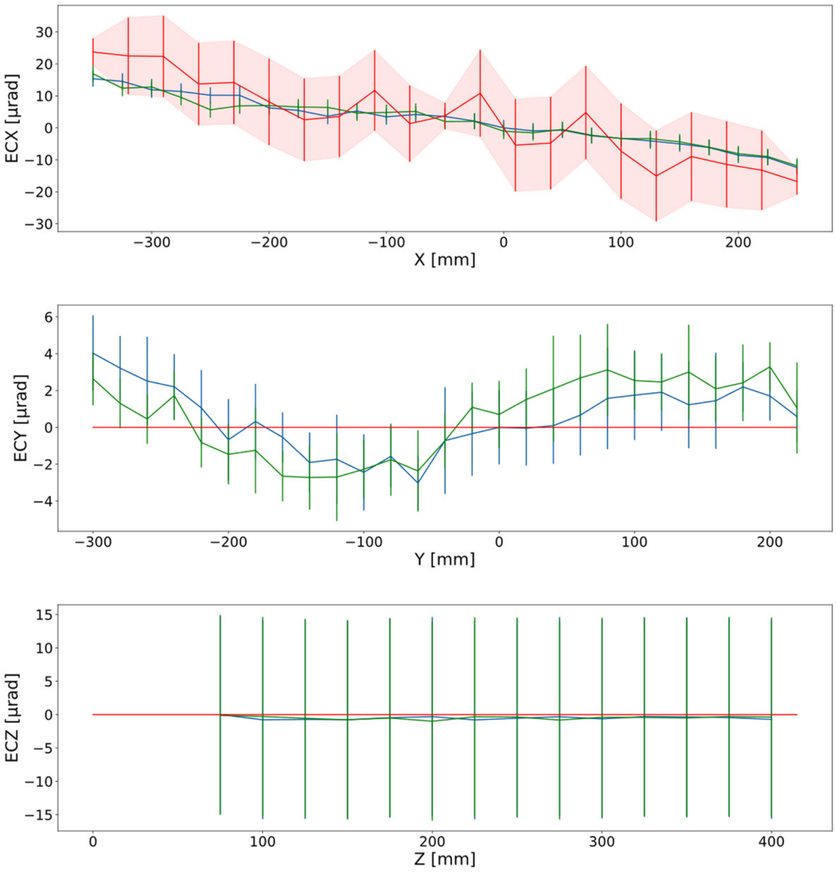
ECX [µrad]
30
20
10
0
−10
−20
−30
−300
−200
−100
0
100
200
X [mm]
ECY [µrad]
6
4
2
0
−2
−4
−300
−200
−100
0
100
200
Y [mm]
ECZ [µrad]
15
10
5
0
−5
−10
−15
0
100
200
300
400
Z [mm]

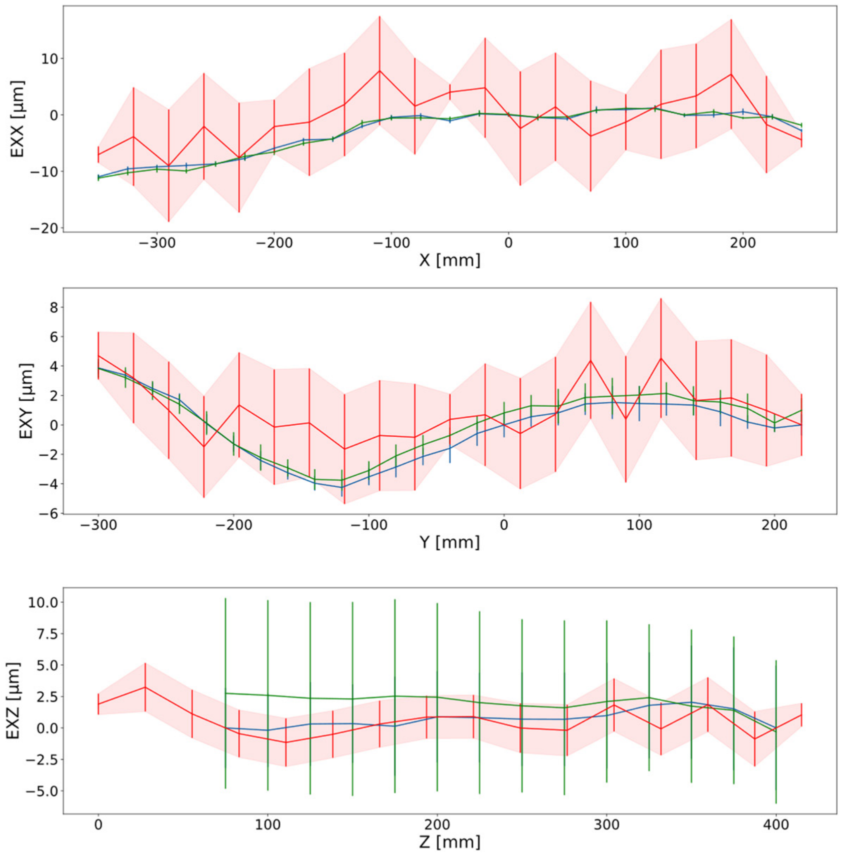
EXX [µm]
10
0
−10
−20
−300
−200
−100
0
100
200
X [mm]
EXY [µm]
8
6
4
2
0
−2
−4
−6
−300
−200
−100
0
100
200
Y [mm]
EXZ [µm]
10.0
7.5
5.0
2.5
0.0
−2.5
−5.0
0
100
200
300
400
Z [mm]

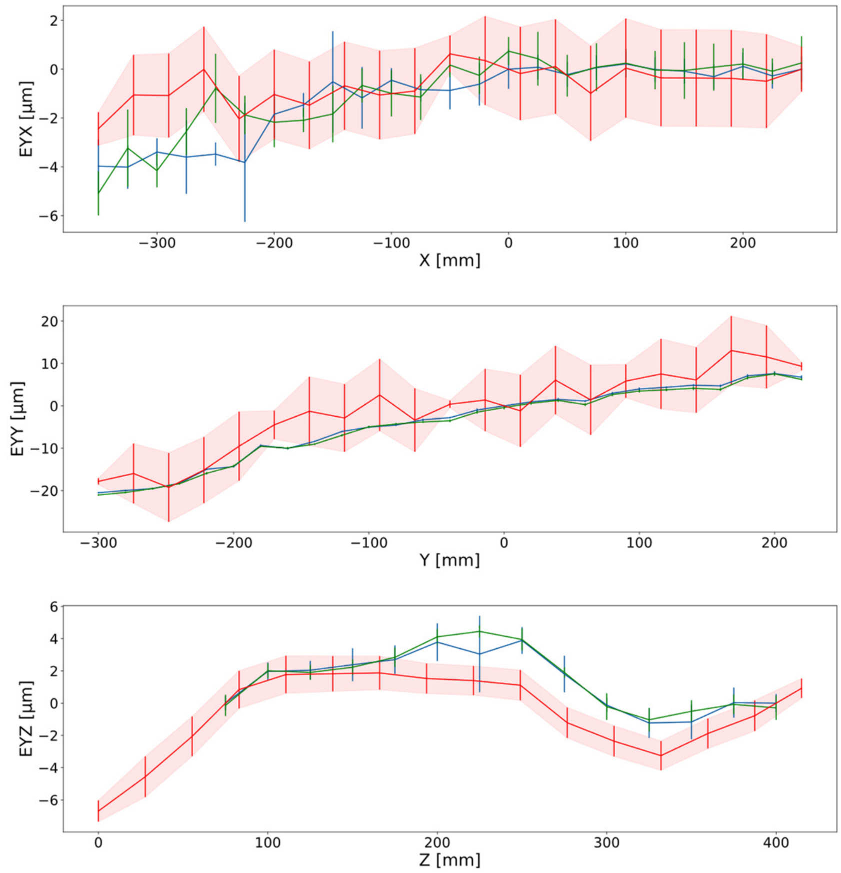
EYX [µm]
2
0
−2
−4
−6
−300
−200
−100
0
100
200
X [mm]
EYY [µm]
20
10
0
−10
−20
−300
−200
−100
0
100
200
Y [mm]
EYZ [µm]
6
4
2
0
−2
−4
−6
0
100
200
300
400
Z [mm]

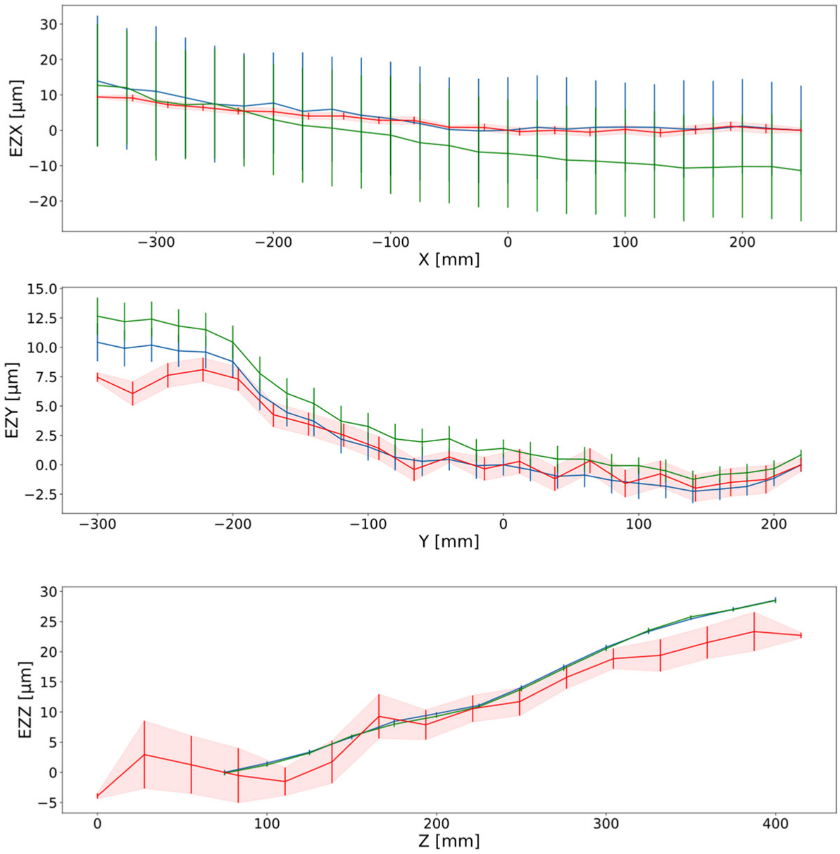

References

1. Schwenke, H.; Knapp, W.; Haitjema, H.; Weckenmann, A.; Schmitt, R.; Delbressine, F. Geometric error measurement and compensation of machines—An update. *CIRP Ann.* **2008**, *57*, 660–675. [CrossRef]
2. Shagluf, A.; Longstaff, A.P. Maintenance strategies to reduce downtime due to machine positional errors. In *Proceedings of the Maintenance Performance Measurement and Management (MPMM) Conference 2014, Coimbra, Portugal, 4–5 September 2014*; Farinha, J.T., Galar, D., Eds.; Imprensa da Universidade de Coimbra: Coimbra, Portugal, 2014; pp. 111–118.
3. Montavon, B.; Dahlem, P.; Peterek, M.; Schmitt, R.H. A Digital Perspective on Machine Tool Calibration. *Int. J. Autom. Technol.* **2020**, *14*, 360–368. [CrossRef]
4. Ibaraki, S.; Knapp, W. Indirect Measurement of Volumetric Accuracy for Three-Axis and Five-Axis Machine Tools: A Review. *Int. J. Autom. Technol.* **2012**, *6*, 110–124. [CrossRef]
5. *ISO/TR 230-11:2018*; Test Code for Machine Tools—Part 11: Measuring Instruments Suitable for Machine Tool Geometry Tests. ISO: Geneva, Switzerland, 2018.
6. Mchichi, N.A.; Mayer, J. Axis Location Errors and Error Motions Calibration for a Five-axis Machine Tool Using the SAMBA Method. *Procedia CIRP* **2014**, *14*, 305–310. [CrossRef]
7. Weikert, S. R-Test, a New Device for Accuracy Measurements on Five Axis Machine Tools. *CIRP Ann.* **2004**, *53*, 429–432. [CrossRef]
8. Brecher, C.; Behrens, J.; Klatte, M.; Lee, T.H.; Tzanetos, F. Measurement and analysis of thermo-elastic deviation of five-axis machine tool using dynamic R-test. *Procedia CIRP* **2018**, *77*, 521–524. [CrossRef]
9. Dahlem, P.; Montavon, B.; Peterek, M.; Schmitt, R.H. Enhancing Laser Step Diagonal Measurement by Multiple Sensors for Fast Machine Tool Calibration. *J. Mach. Eng.* **2018**, *18*, 64–74. [CrossRef]
10. Li, H.; Zhang, P.; Deng, M.; Xiang, S.; Du, Z.; Yang, J. Volumetric error measurement and compensation of three-axis machine tools based on laser bidirectional sequential step diagonal measuring method. *Meas. Sci. Technol.* **2020**, *31*, 55201. [CrossRef]
11. Mutilba, U.; Yagüe-Fabra, J.A.; Gomez-Acedo, E.; Kortaberria, G.; Olarra, A. Integrated multilateration for machine tool automatic verification. *CIRP Ann.* **2018**, *67*, 555–558. [CrossRef]
12. Schwenke, H.; Schmitt, R.; Jatzkowski, P.; Warmann, C. On-the-fly calibration of linear and rotary axes of machine tools and CMMs using a tracking interferometer. *CIRP Ann.* **2009**, *58*, 477–480. [CrossRef]
13. Lau, K.; Liu, Y.; Qiao, G.; Xie, L. Volumetric Error Compensation System with Laser Tracker and Active Target. US-20100176270-A1. 2010. Available online: https://image-ppubs.uspto.gov/dirsearch-public/print/downloadPdf/20100176270 (accessed on 1 January 2023).

14. Montavon, B.L.; Dahlem, J.P.; Schmitt, R.H. Fast Machine Tool Calibration using a single Laser Tracker. In *Laser Metrology and Machine Performance XIII 13th International Conference and Exhibition on Laser Metrology, Machine Tool, CMM & Robotic Performance Lamdamap 2019*; Blunt, L., Knapp, W., Eds.; Cranfield University Campus: Bedfordshire, UK, 2019; pp. 203–213.
15. Aguado, S.; Samper, D.; Santolaria, J.; Aguilar, J.J. Volumetric verification of multiaxis machine tool using laser tracker. *Sci. World J.* **2014**, *2014*, 959510. [CrossRef] [PubMed]
16. Kabsch, W. A solution for the best rotation to relate two sets of vectors. *Acta Cryst A* **1976**, *32*, 922–923. [CrossRef]
17. Schönemann, P.H. A generalized solution of the orthogonal procrustes problem. *Psychometrika* **1966**, *31*, 1–10. [CrossRef]
18. Esmaeili, S.; Mayer, R.; Sanders, M.; Dahlem, P.; Xing, K. Five-axis machine tool volumetric and geometric error reduction by indirect geometric calibration and lookup tables. *J. Manuf. Sci. Eng.* **2021**, 1–25. [CrossRef]
19. *JCGM 102:2011*; Evaluation of Measurement Data–Supplement 2 to the "Guide to the Expression of Uncertainty in Measurement"–Extension to Any Number of Output Quantities. BIPM: Sèvres, France, 2011.
20. *JCGM 100:2008*; Evaluation of Measurement Data—Guide to the Expression of Uncertainty in Measurement. BIPM: Sèvres, France, 2008.
21. Montavon, B.; Dahlem, P.; Schmitt, R. Effektive Analyse von Werkzeugmaschinenkalibrierdaten*/Effective analysis of machine tool calibration data. VoluSoft as a showcase for user-friendly visualization and processing of machine tool calibration data. *Wt Werkstattstechnik Online* **2018**, *108*, 755–759. [CrossRef]

Disclaimer/Publisher's Note: The statements, opinions and data contained in all publications are solely those of the individual author(s) and contributor(s) and not of MDPI and/or the editor(s). MDPI and/or the editor(s) disclaim responsibility for any injury to people or property resulting from any ideas, methods, instructions or products referred to in the content.